Aspect Angle Classification via Physically Realizable Matched Illumination Waveform Design

Jennifer E. Quirk[1], Matthew B. Heintzelman[1], Daniel B. Herr[1],
Patrick M. McCormick[1], Shannon D. Blunt[1], Brianna Maio[2]
[1]Radar Systems Lab (RSL), University of Kansas, Lawrence, KS
[2]Sandia National Laboratories (SNL), Albuquerque, NM

***Abstract*—Matched illumination waveform design seeks to improve classification and detection performance by leveraging *a priori* information about the expected scattering from the illuminated environment. This approach leads to a waterfilling solution, in which more power is allocated to high-SNR frequency channels, resulting in improved discrimination capabilities. While much research has been devoted to the derivation and design of matched illumination waveforms, the question remains of how much benefit is obtained by the matched illumination approach. In the context of physical waveforms, we compare the classification and detection performance of matched illumination waveforms to that of traditional optimized RFM waveforms. The relative capability of MI is examined via Monte Carlo simulation, where the simulated test object consists of simulated azimuth-dependent scattering characteristics of a Toyota Camry.**

***Index Terms*—matched illumination, mutual information, waveform diversity**

I. Introduction

Due to advances in radar transmit architectures, radar waveform optimization has become an increasingly deep field of research, with a plethora of solutions provided for varied application spaces. Significantly, physically-realizable optimal waveforms have been posed seeking to minimize range-sidelobe-induced self-interference [1], [2], perform spectral deconfliction [3], and provide combined radar/communications functionality [4], [5]. In each of these cases, the assumption is that the probing sensor maintains high enough SNR that the waveform correlation error (e.g. sidelobes) is greater than random errors due to receiver noise. Somewhat less attention has been paid to the problem of designing optimal physical waveforms for radars operating in adverse conditions, where the input SNR may be low.

The seminal work of Mark Bell [6] introduced information-theoretic waveform design methods for detection and classification of extended scattering profiles. Bell's optimal detection waveforms seek to maximize the signal-to-noise ratio (SNR) at the output of the radar receiver for a known scattering response. This approach leads to an eigenvector solution, which has also been applied to the target identification problem [7], [8]. Bell's optimal estimation waveforms maximize the mutual information between an ensemble of expected scattering responses and the received radar signal. This ensemble-based approach lends itself to waveform design in a high-resolution radar (HRR) context, in which target identification is especially sensitive to the radar-target orientation [9], [10]. These optimal estimation waveforms are deemed "matched illumination" (MI) waveforms, since the design procedure seeks to match the waveforms to the illuminated environment.

Much research has been devoted to the design and analysis of Bell's optimal estimation waveforms. A significant contribution lies in [11], which derives the optimal detector for the optimal estimation waveforms. In terms of implementation, constant modulus and spectral containment constraints have been imposed on the optimal estimation waveform design formulation [12], [13] so that the resulting waveforms are conducive to physical realization in RF hardware. An outline of alternative MI waveform design metrics is provided in [14], and [15] uses a gradient-based approach for an ensemble that follows a Gaussian mixture model. Detection via sequential hypothesis testing is examined in [16], which poses MI waveform design in a cognitive radar context. Another overview of MI is given in [17].

Here, a physically-realizable implementation of MI waveforms is presented, followed by a discussion of a framework for sequential classification and detection stages. The MI waveform design procedure is simulated for an ensemble consisting of angle-varying HRR scattering profiles of a Toyota Camry. Further simulation results examine the classification and detection performance of the MI waveforms relative to that of traditional optimized RFM waveforms. Comparisons of classification and detection capability obtained from this simulation are used to determine the benefit of MI design over traditional RFM waveform design.

II. Radar Signal Model & Matched Filtering

The goal of MI waveform design is to leverage *a priori* information about the observed scattering scene to improve detection and classification performance over that achieved by traditional radar waveforms. To understand the impact of the chosen waveform design procedure on a subsequent estimate of the scene, it is imperative to examine the signal model. Given an ensemble of L possible time-domain scattering profiles $\{g_{\ell(t)}\}$ for $\ell = 1, 2, ..., L$, the received radar signal is modeled as a linear convolution process with additive noise, which is described as

$$y(t) = \alpha(s(t) * \bar{g}(t)) + n(t) \tag{1}$$

This work was supported by Sandia National Laboratories under Contract #2415977. DISTRIBUTION STATEMENT A. Approved for public release.

where $\bar{g}(t) \in \{g_{\ell(t)}\}$, $n(t)$ is complex-valued additive white Gaussian noise (AWGN), and α is a scalar herein modeled as a zero-mean and unit-variance complex normal random variable.

To classify the true delay profile $\bar{g}(t)$ from the set of hypotheses, estimation is performed via matched filtering. Since it is assumed that the true scattering profile exists in the set of hypotheses, define $\bar{y}_\ell(t)$ as the ideal received signal corresponding to the ℓth profile, such that

$$\bar{y}_\ell(t) = s(t) * g_\ell(t), \tag{2}$$

which results in the matched filter expression

$$h_\ell(t) = s^*(-t) * g_\ell^*(-t). \tag{3}$$

Then, the matched filter estimate is

$$\begin{aligned} z_\ell(t) &= h_{\mathrm{MF},\ell}(t) * y(t)dt \\ &= [s^*(-t) * g_\ell^*(-t)] * [\alpha(s(t) * \bar{g}(t)) + n(t)], \end{aligned} \tag{4}$$

or in the frequency domain (taking the Fourier transform),

$$\begin{aligned} Z_\ell(f) &= [S^*(f)G_\ell^*(f)] \cdot [\alpha S(f)\bar{G}(f) + N(f)] \\ &= |S(f)|^2\bar{G}(f)G_\ell^*(f) + S^*(f)G_\ell^*(f)N(f). \end{aligned} \tag{5}$$

From (4) and (5), the matched filter estimate of the true scattering profile is corrupted by waveform artifacts (from transmission/matched filtering) as well as noise. Mismatched filtering [18]–[20] may be effective at minimizing these waveform artifacts at the cost of SNR loss, which may be undesirable if already SNR-limited. Since the purpose of MI is to improve detection/classification by transmitting only in "good" spectral channels (those that are not SNR-limited), only matched filter processing is considered here to avoid further SNR penalty.

III. MI Waveform Design

A. Background

The optimal estimation waveforms from [6] leverage *a priori* knowledge of the expected scattering to achieve improved classification performance. From an information theoretic perspective, if the mutual information between the matched filter estimate from (5) and the ensemble of spectral profiles characterizing the expected scattering is higher, then classification is more accurate. To this end, these optimal estimation waveforms have the following PSD:

$$P(f) = \max\left\{0, A - \frac{\sigma_n^2}{\sigma_G^2(f)}\right\}, \tag{6}$$

where σ_n^2 is the noise power (assuming white Gaussian noise), $\sigma_G^2(f)$ is the spectral profile variance, and the scalar A is determined via the following signal energy constraint

$$\int_{-B/2}^{B/2} P(f)df - E_s = 0, \tag{7}$$

where B is the signal bandwidth, and E_s is the signal energy.

The implication of (6) is that MI waveform design requires a significant amount of prior knowledge of scattering characteristics, which may not be possible to obtain in practice. Explicitly, (6) requires knowledge of the spectral variation among the hypothesized scattering profiles (which may be significant [21]) as a function of frequency. The required prior information is further compounded through dependence on other factors such as azimuth angle, elevation angle, and SNR. If all of these are known, then the solution to (6) follows a waterfilling approach, whereby more power is allocated to frequencies at which the variance across the ensemble of spectral profiles is significant, relative to the noise power.

B. Implementation

The detection/classification problem presented here considers a single stationary object that may or may not be present in the scene, which is being illuminated by a monostatic radar. It is assumed that the elevation angle to the region of interest is known, but the range and azimuth angle between the region of interest and platform are unknown. Therefore, the ensemble of expected scattering $\{G_\ell(f)\}$ consists of spectral profiles of the object for each possible azimuth angle (indexed by ℓ), with classification being performed in the frequency domain for computational convenience.

Since the range to the object is unknown, we introduce a random phase rotation on each spectral profile as

$$\tilde{G}_\ell(f) = G_\ell(f)e^{j\varphi_\ell}. \tag{8}$$

Assuming that φ_ℓ is a random phase that is uniformly distributed on $[0, 2\pi)$, the frequency-dependent mean of each profile $\tilde{\mu}_\ell(f)$ is zero, so the sample variance across ensemble of spectral profiles simplifies as

$$\begin{aligned} \sigma_G^2(f) &= \frac{1}{L}\sum_{\ell=0}^{L-1} |\tilde{G}_\ell(f) - \tilde{\mu}_\ell(f)|^2 \\ &= \frac{1}{L}\sum_{\ell=0}^{L-1} |G_\ell(f)|^2. \end{aligned} \tag{9}$$

In the particular implementation considered here, the $G_\ell(f)$ are normalized to unit energy so that each has equal impact in (9). This step is especially important for profiles that are comprised of just a few dominant scatterers.

It is convenient to reformulate (6) to explicitly include a spectral taper $W(f)$ [23] as a means of enforcing spectral containment of the optimized waveforms via

$$\tilde{P}(f) = \max\left\{0, W(f)\left(A - \frac{\sigma_n^2}{\sigma_G^2(f)}\right)\right\}, \tag{10}$$

which necessitates replacing $P(f)$ with $\tilde{P}(f)$ in (7). The template from (10) and its corresponding signal energy constraint from (7) are evaluated in tandem using MATLAB's *fzero* [22] function to simultaneously determine the signal energy required to achieve an expected SNR and the scalar A to satisfy the constraint. This numerical approach is necessary since $\sigma_G^2(f)$ may not have an analytical form. The final template is then provided to the pseudo-random optimized FM (PRO-FM) waveform design framework [24], which leverages repeated time-frequency alternating projections to produce physically realizable waveforms having a prescribed spectral shape.

IV. Profile Classification

The statistic leveraged for profile classification is a normalized version of the matched filter response. Selecting the zero-lag instant of (4), define the normalized correlation coefficient ρ_ℓ^2 as

$$\rho_\ell^2 = \frac{|z_\ell(0)|^2}{\|y(t)\|^2 \|g_\ell(t)\|^2}, \tag{11}$$

which may be equivalently stated in the frequency domain, via Parseval's Theorem, as

$$\rho_\ell^2 = \frac{\left| \int_{-\infty}^{\infty} G_\ell(f) Y(f) df \right|^2}{\|Y(f)\|^2 \|G_\ell(f)\|^2}. \tag{12}$$

This approach is consistent with that of the adaptive coherence estimator (ACE) [25], [26], which measures coherence while remaining invariant to scaling of the input vectors.

Rather than developing an optimal L-hypothesis classifier, it is more efficient to first calculate ρ_ℓ^2 for all $\ell \in 1, 2, ..., L$, choose the maximally correlated profile, and then consider a case of binary detection in which the noise-only hypothesis is considered. This methodology separates the classification problem into two stages: 1) classification based on the maximization of (12), and 2) detection of the maximally correlated hypothesis. For the classification stage, there are L hypotheses, defined as

$$H_\ell : Z(f) = |S(f)|^2 G_\ell(f) + S^*(f) N(f) \qquad \ell = 1, 2, ..., L. \tag{13}$$

Classification is performed by determining

$$\hat{\ell} = \underset{\ell}{\operatorname{argmax}} \{\rho_\ell^2\} \tag{14}$$

corresponding to spectral profile $G_{\hat{\ell}}(f)$. The maximum correlation coefficient $\rho_{\hat{\ell}}^2$ is then compared to a detection threshold to determine whether or not the hypothesized object is actually present in the scene.

The profile classification leads to a binary detection stage, which consists of two hypotheses

$$\begin{aligned} H_0 &: Z(f) = S^*(f) N(f) \\ H_1 &: Z(f) = |S(f)|^2 G_{\hat{\ell}}(f) + S^*(f) N(f), \end{aligned} \tag{15}$$

where $G_{\hat{\ell}}(f)$ is obtained from the procedure in (14). Assuming that, in the target-present case, the observed profile is correctly classified, the likelihood ratio test (LRT) may be stated as

$$\frac{P(\rho_\ell^2 | H_1)}{P(\rho_\ell^2 | H_0)} \underset{H_0}{\overset{H_1}{\gtrless}} \gamma, \tag{16}$$

where γ is the detection threshold for the LRT. The threshold is found by solving the integral equation

$$P_{FA} = \int_0^\gamma P(\rho_\ell^2 | H_0) d\rho_\ell^2 \tag{17}$$

for γ. Due to the normalization in (12), the likelihood functions for each hypothesis are not straightforward to compute and integrate. As such, (17) is solved approximately via Monte Carlo methods that are discussed in the following section.

V. Monte Carlo Simulation

A. Waveform Design

The object of interest considered here for classification is a Toyota Camry, whose scattering characteristics have been obtained from [27]. This dataset consists of spectral profiles for azimuth angles between $0.0625°$ and $360°$, spaced by $0.0625°$, for a $30°$ elevation angle. Fig. 1 shows the normalized correlation between the spectral profiles as a function of azimuth angle. The Camry exhibits symmetric structures, most notably in the prominent correlation along the anti-diagonal. Moreover, the main diagonal has some azimuthal width, indicating that the correlation length of the Camry is greater than $0.0625°$ (that is, the data is spatially oversampled).

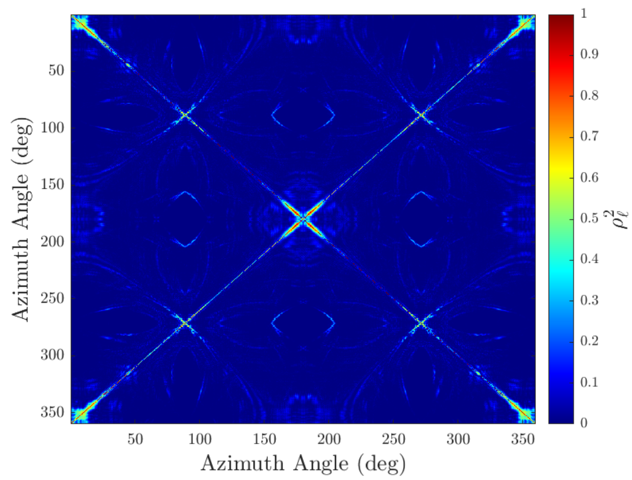

Fig. 1. Correlation between Camry spectral profiles as a function of azimuth angle

Fig. 2 shows the spectral variance $\sigma_G^2(f)$, obtained via (9), along with the single spectral profile at $\phi = 46°$ (corresponding to $\ell = 10$) for the Camry. The spectral variance trends downward as a function of frequency, which is supported by the observation that most of the power in the $\phi = 46°$ profile is allocated at the lower frequencies. Thus, we should expect the MI waveform design procedure to allocate most of the power to the lower frequencies, since this is where the spectral variance is the highest.

As a proof-of-concept for assessing the efficacy of MI waveform design, in comparison with traditional RFM waveform optimization [24], a high-dimensional Monte Carlo simulation was constructed. The simulation varies the noise $n(t)$ and scattering coefficient α from (1), as well as the waveform initialization provided to both the MI and traditional RFM design procedures. Since highly correlated profiles may not be readily distinguished, as well as for Monte Carlo runtime considerations, the ensemble used for the MI waveform design consists only of profiles between azimuth angles $10°$ and $86°$, spaced by $4°$ (20 profiles total).

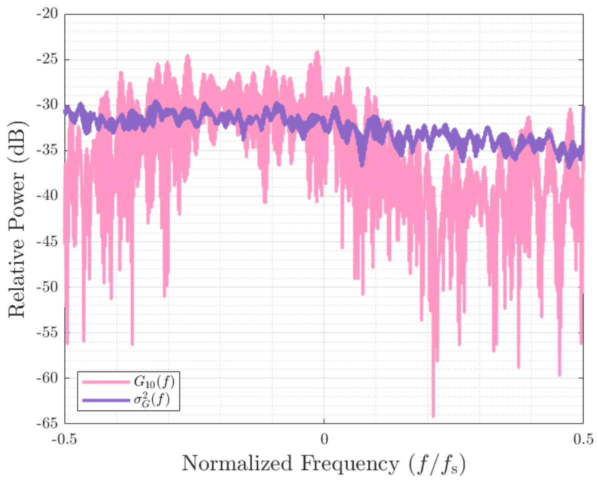

Fig. 2. Spectral variance $\sigma_G^2(f)$ via (9) and single spectral profile $G_{10}(f)$

Fig. 3 shows the MI PSD templates, obtained via (10), for various SNRs, where $W(f)$ is a super-Gaussian taper with exponent 32 [28] to provide good spectral containment. Here, SNR is specified before matched filtering, and the templates have been energy-normalized for plotting purposes to facilitate comparison. For the high-SNR case (magenta trace), the MI PSD template approaches $W(f)$ since, via (10), fewer of the frequency bins are noise-limited, and so each receives a power near A. As the SNR degrades (remaining traces), the noise begins to dominate (most notable towards the right-hand portion of the spectra), so no power is allocated to these portions of the templates. However, due to the signal energy constraint in (7), when a narrower spectrum is used, more relative power is available to allocate towards spectral locations with higher SNR.

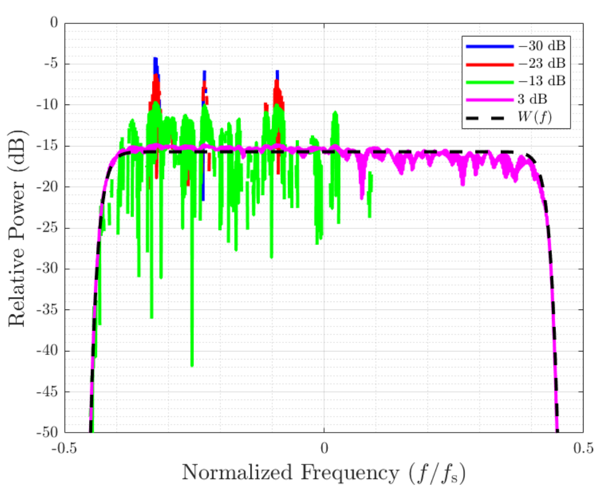

Fig. 3. PSD templates via (10) for various SNRs

B. Detection & Classification

To ascertain the benefit of MI, the same simulation is repeated for MI waveforms designed to (10) and traditional RFM waveforms designed via PRO-FM to match the super-Gaussian taper $W(f)$, which has a 3 dB bandwidth of approximately 4.5 GHz. The Camry is placed at a range of 8 km, with the assumption that this range is known (obtained from GPS/INS data in a practical scenario) to within a range bin. The simulation presented here emulates a spotlight mode collect at an elevation angle of 30° for azimuth angles between 10° and 86°, separated by 4° (same as the MI design ensemble). At each azimuth angle, a single waveform of each type is transmitted. The simulation is repeated 5000 times, where SNR is specified prior to matched filtering.

Fig. 4 shows the normalized correlation coefficient from (11) for a single run as a function of azimuth angle for the MI waveforms and the regular PRO-FM waveforms at truth azimuth angle $\phi = 46°$ and -13 dB SNR. The MI case exhibits some correlation to non-truth profiles since the waveforms are designed to an ensemble of all profiles, with the correlation to the truth profile being especially high. However, this correlation to non-truth profiles may lead to incorrect classification; in Fig. 4, the correlation coefficient at $\phi = 78°$ is quite high (relative to the maximum) and therefore could produce an incorrect classification in a different run. For regular PRO-FM, correlation to the non-truth profiles is generally slightly lower, but so is correlation to the truth profile.

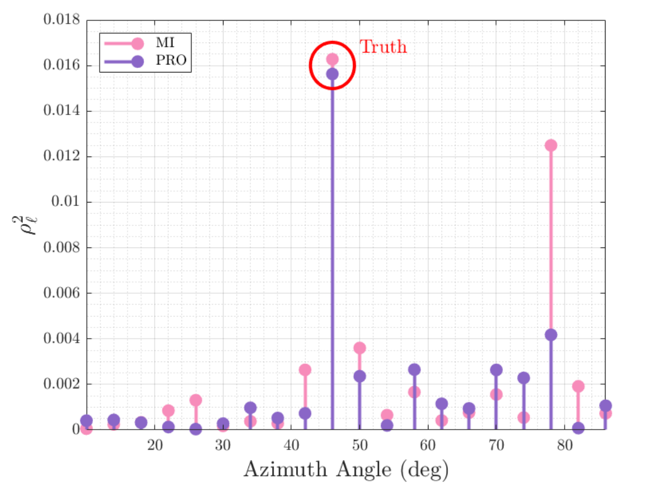

Fig. 4. Normalized correlation coefficient ρ_ℓ^2 via (12) for MI and regular PRO-FM at azimuth angle $\phi = 46°$ and -13 dB input SNR

Fig. 5 shows the classification rate for the MI and regular PRO-FM cases as a function of azimuth angle for various SNRs. The traces show that, for low input SNRs, MI waveforms generally provide slightly improved classification performance, relative to that of PRO-FM. For the high-SNR case (magenta trace), both MI and regular PRO-FM perform correct classification nearly all the time for all angles. As SNR degrades, the classification rate degrades as well, becoming quite poor at -30 dB, with an average classification rate of 21% and 19% for MI and regular PRO-FM, respectively. Moreover, for the lower SNRs, the classification rate varies across azimuth angle, with this variation being more sigificant for the MI case than the regular PRO-FM case. This is again due to the fact that the MI waveforms are designed to an ensemble of all profiles, and it is possible that one profile with dramatically different scattering characteristics could skew the design template.

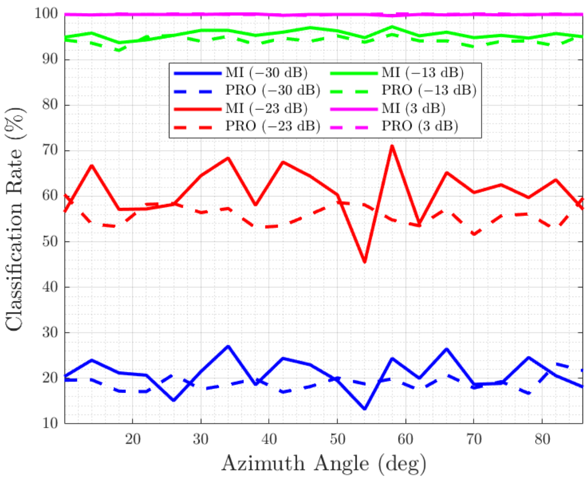

Fig. 5. Classification rate as a function of azimuth angle for MI and regular PRO-FM, where the SNRs specified in parentheses are measured prior to matched filtering

The average classification rates obtained via simulation are summarized in Table I. These results indicate a quantitative improvement in the classification rates for the MI waveforms when compared to regular PRO-FM at the same SNR. While the average classification rates are nearly identical for the 3 dB SNR case, MI achieves 5% better classification, on average, than regular PRO-FM for the -23 dB SNR. Though less dramatic, MI also outperforms regular PRO-FM for the -30 dB and -13 dB SNRs, achieving 2% and 1.3% average improvement, respectively.

TABLE I
AVERAGE CLASSIFICATION RATE ACROSS AZIMUTH ANGLE FOR MI AND REGULAR PRO-FM

	MI	PRO
SNR $= -30$ dB	21%	19%
SNR $= -23$ dB	60.9%	55.9%
SNR $= -13$ dB	95.5%	94.2%
SNR $= 3$ dB	99.9%	99.9%

After classification, the binary detection procedure described by (16) and (17) is used to reject possible false alarms due to noise. To solve for the detection threshold in (17), histograms of ρ_ℓ^2 are formed from the Monte Carlo data discussed above, which are then leveraged to approximate the likelihood functions $P(\rho_\ell^2|H_1)$ and $P(\rho_\ell^2|H_0)$. The histograms for the input SNRs of -23 dB and -13 dB are depicted in Figs. 6 and 7, respectively. For both SNRs, the histograms indicate that the distributions of ρ_ℓ^2 corresponding to the target-present hypothesis are shifted slightly to the right for the MI case compared to the regular PRO-FM case. Despite this, the distributions for the null hypotheses are nearly identical for both waveform classes and both SNRs. Consequently, improved detection results are achieved for the MI waveforms.

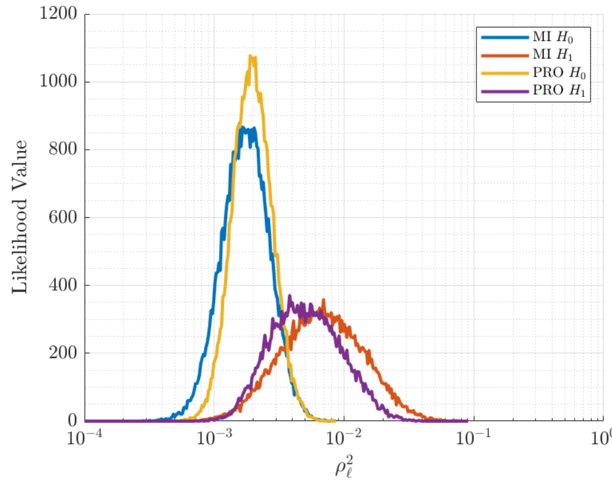

Fig. 6. Histograms of ρ_ℓ^2 via (12), formed from the Monte Carlo data for an input SNR of -23 dB

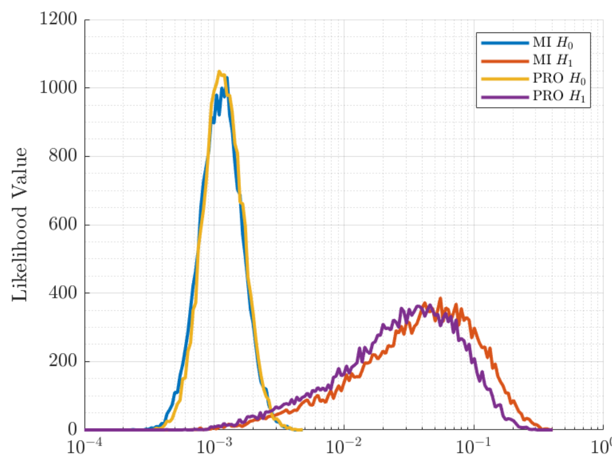

Fig. 7. Histograms of ρ_ℓ^2 via (12), formed from the Monte Carlo data for an input SNR of -13 dB

From the histograms depicted in Figs. 6 and 7, (17) can be used to approximately solve for the detection threshold γ. With this threshold, a binary detection problem is constructed according to (16). The resulting receiver operating characteristic (ROC) curves generated via this procedure are shown in Fig. 8. For the lower SNRs, the ROCs clearly demonstrate the improved detection capability provided by the MI waveforms, when compared to regular PRO-FM. Fig. 8, combined with Fig. 5, suggests that prior knowledge of the SNR, as well as the scattering characteristics of the scene, can be leveraged to improve the classification and detection capabilities of a radar system.

VI. CONCLUSIONS

The benefit of MI waveform design for scattering profile classification has been examined in simulation using physically realizable random FM (RFM) waveforms. MI can provide enhanced classification capability relative to RFM waveforms

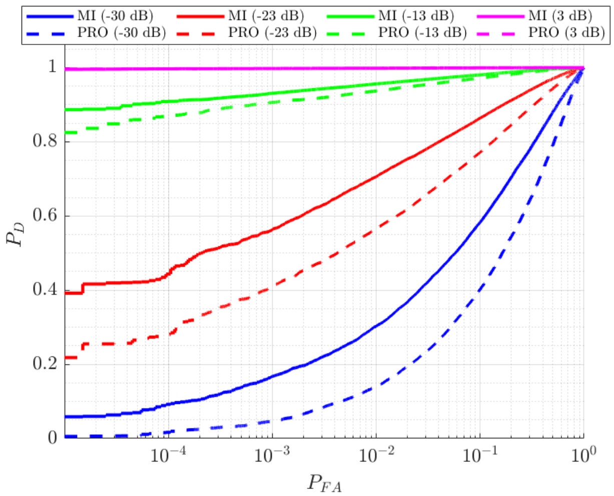

Fig. 8. ROCs for MI and regular PRO-FM at various input SNRs

optimized only for general spectral containment. This benefit arises primarily in low-SNR scenarios, where the waterfilling solution for MI uses only a small portion of the available bandwidth, improving the SNR for frequency bins where the *a priori* profiles are most different. This SNR-based allocation emphasizes discrimination capability within the design profile ensemble. Incorporation of the PRO-FM spectral shaping method into the MI waveform design ensures that the realized waveforms meet the FM structure requirements making them amenable to high-power transmitters. Furthermore, incorporation of a spectral taper into the MI template ensures that the implemented waveforms are spectrally contained and therefore physically realizable.

References

[1] C. A. Mohr, P. M. McCormick, C. A. Topliff, S. D. Blunt, J. M. Baden, “Gradient-based optimization of PCFM radar waveforms,” *IEEE Trans. Aerospace & Electronic Systems*, vol. 57, no. 2, pp. 935-956, Apr. 2021.

[2] B. White, M. B. Heintzelman, S. D. Blunt, “Alternative ‘bases’ for gradient-based optimization of parameterized FM radar waveforms,” *IEEE Radar Conf.*, San Antonio, TX, May 2023.

[3] J. W. Owen, C. A. Mohr, B. H. Kirk, S. D. Blunt, A. F. Martone, K. D. Sherbondy, “Demonstration of real-time cognitive radar using spectrally-notched random FM waveforms,” *Intl. Radar Conf.*, Washington, DC, Apr. 2020.

[4] B. Ravenscroft, A. Fontes, P. M. McCormick, S. D. Blunt, C. Musgrove, “Physically realizable multi-user radar/communications (MuRC),” *IEEE Radar Conf.*, San Antonio, TX, May 2023.

[5] B. Ravenscroft, P. M. McCormick, S. Blunt, E. S. Perrins, C. Sahin, J. G. Metcalf, “Experimental assessment of tandem-hopped radar and communications (THoRaCs),” *Intl. Radar Conf.*, Toulon, France, Sept. 2019.

[6] M. R. Bell, “Information theory and radar waveform design,” *IEEE Trans. Information Theory*, vol. 39, no. 5, pp. 1578-1597, Sept. 1993.

[7] S. U. Pillai, H. S. Oh, D. C. Youla, J. R. Guerci, “Optimal transmit-receiver design in the presence of signal-dependent interference and channel noise,” *IEEE Trans. Information Theory*, vol. 46, no. 2, pp. 577-584, March 2000.

[8] J. R. Guerci, S. U. Pillai, “Theory and application of optimum transmit-receive radar,” *Intl. Radar Conf.*, Alexandria, VA, May 2000.

[9] R. A. Mitchell, J. J. Westerkamp, “Robust statistical feature based aircraft identification,” *IEEE Trans. Aerospace & Electronic Systems*, vol. 35, no. 3, pp. 1077-1094, July 1999.

[10] S. P. Jacobs, J. A. O’Sullivan, “Automatic target recognition using sequences of high resolution radar range-profiles,” *IEEE Trans. Aerospace & Electronic Systems*, vol. 36, no. 2, pp. 364-381, April 2000.

[11] S. Kay, “Optimal signal design for detection of Gaussian point targets in stationary Gaussian clutter/reverberation,” *IEEE Journal of Selected Topics in Signal Processing*, vol. 1, no. 1, pp. 31-41, June 2007.

[12] J. Bae, N. A. Goodman, “Evaluation of modulus-constrained matched illumination waveforms for target identification,” *IEEE Radar Conf.*, Arlington, VA, 2010.

[13] K. Adhikari, D. A. Hague, “Matched illumination waveforms using multi-tone sinusoidal frequency modulation,” *IEEE Statistical Signal Processing Workshop*, Rio de Janeiro, Brazil, 2021.

[14] R. A. Romero, J. Bae, N. A. Goodman, “Theory and application of SNR and mutual information matched illumination waveforms,” *IEEE Trans. Aerospace & Electronic Systems*, vol. 47, no. 2, pp. 912-927, April 2011.

[15] Y. Gu, N. A. Goodman, “Information-theoretic waveform design of Gaussian mixture radar target profiling,” *IEEE Trans. Aerospace & Electronic Systems*, vol. 55, no. 3, pp. 1528-1536, June 2019.

[16] N. A. Goodman, P. R. Venkata, M. A. Neifeld, “Adaptive waveform design and sequential hypothesis testing for target recognition with active sensors,” *IEEE Journal of Selected Topics in Signal Processing*, vol. 1, no. 1, pp. 105-113, June 2007.

[17] D. T. Djessing, *Target Adaptive Matched Illumination Radar: Principles and Applications*, London, UK: Peter Peregrinus Ltd., 1986.

[18] M. H. Ackroyd, F. Ghani, “Optimum mismatched filters for sidelobe suppression,” *IEEE Trans. Aerospace & Electronic Systems*, vol. AES-9, no. 2, pp. 214-218, March 1973.

[19] C. C. Jones, S. D. Blunt, “Mismatched complementary-on-receive filtering of diverse FM waveform subsets,” *Intl. Radar Conf.*, Toulon, France, Sept. 2019.

[20] A. W. Doerry, “Catalog of window taper functions for sidelobe control,” Sandia Technical Report, SAND2017-4042, Apr. 2017.

[21] M. A. Richards, *Fundamentals of Radar Signal Processing*. New York City, NY: McGraw-Hill, 2022.

[22] https://www.mathworks.com/help/matlab/ref/fzero.html

[23] D. B. Herr, “Information theoretic waveform design with application to physically realizable adaptive-on-transmit radar,” Ph.D. dissertation, University of Kansas, Lawrence, KS, 2024.

[24] J. Jakabosky, S. D. Blunt, B. Himed, “Spectral-shape optimized FM noise radar for pulse agility,” *IEEE Radar Conf.*, Philadelphia, PA, May 2016.

[25] L. L. Scharf, L. T. McWhorter, “Adaptive matched subspace detectors and adaptive coherence estimators,” *30th Asolimar Conf. on Signals, Systems, & Computers*, Pacific Grove, CA, 1996, pp. 1114-1117, vol. 2.

[26] L. T. McWhorter, L. L. Scharf, L. J. Griffiths, “Adaptive coherence estimation for radar signal processing,” *30th Asolimar Conf. on Signals, Systems, & Computers*, Pacific Grove, CA, 1996, pp. 536-540, vol. 1.

[27] https://www.sdms.afrl.af.mil/index.php?collection=cv_dome

[28] C. A. Mohr, S. D. Blunt, “Designing random FM radar waveforms with compact spectrum,” *IEEE International Conference on Acoustics, Speech, & Signal Processing*, Toronto, ON, Canada, 2021.